

## Research



**Cite this article:** Lee K, Xie J, Park H, Jung H, Oh J-M. 2023 Controlled molecular arrangement of easily aggregated deoxycholate with layered double hydroxide. *R. Soc. Open Sci.* **10**: 230506. <https://doi.org/10.1098/rsos.230506>

Received: 23 April 2023

Accepted: 12 September 2023

**Subject Category:**

Chemistry

**Subject Areas:**

materials science

**Keywords:**

deoxycholate, aggregation, layered double hydroxide, molecular arrangement

**Authors for correspondence:**

Hyun Jung

e-mail: [chemphile@dongguk.edu](mailto:chemphile@dongguk.edu)

Jae-Min Oh

e-mail: [jaemin.oh@dongguk.edu](mailto:jaemin.oh@dongguk.edu)

<sup>†</sup>These authors contributed equally to this work. This article has been edited by the Royal Society of Chemistry, including the commissioning, peer review process and editorial aspects up to the point of acceptance.

Electronic supplementary material is available online at <https://doi.org/10.6084/m9.figshare.c.6858282>.



# Controlled molecular arrangement of easily aggregated deoxycholate with layered double hydroxide

Kyoungyoung Lee<sup>1,†</sup>, Jing Xie<sup>2,†</sup>, Hyeonjin Park<sup>2</sup>, Hyun Jung<sup>1</sup> and Jae-Min Oh<sup>2</sup>

<sup>1</sup>Department of Chemistry and <sup>2</sup>Department of Energy and Materials Engineering, Dongguk University, Seoul 04620, Republic of Korea

J-MO, 0000-0003-1638-9957

Deoxycholate (DA) is a natural emulsifying agent involved in the absorption of dietary lipids. Due to the facial distribution of hydrophobic-hydrophilic region, DA easily aggregates under ambient conditions, and this property hinders the practical application of DA in clinical applications. In this study, we found that the molecular arrangement of DA molecules could be controlled by using layered double hydroxide (LDH) under a specific reaction condition. The effect of reaction methods such as co-precipitation, ion exchange and reconstruction on the molecular arrangement of DA was investigated by X-ray diffraction, Fourier-transform infrared spectroscopy, high-resolution transmission electron microscopy and differential scanning calorimetry. It was demonstrated that the self-aggregation of DA molecules could be suppressed by the oriented arrangement of DA between the gallery space of LDH. The DA moiety was well stabilized in the LDH layers due to the electrostatic interaction between DA molecules and LDH layers. The most ordered arrangement of DA molecules was observed when DA was incorporated into LDH via a reconstruction method. The DA molecules arranged in LDH via reconstruction did not show significant exothermic or endothermic behaviour up to 400°C, showing that the DA moiety lost its intermolecular attraction in between LDH layers.

## 1. Introduction

Controlling molecular arrangement has attracted increasing interest in biology-related sciences as the molecular orientation affects various physicochemical properties in addition to the molecule's intrinsic properties. For instance, polymorphism, which refers to two or more crystalline phases of molecules, is

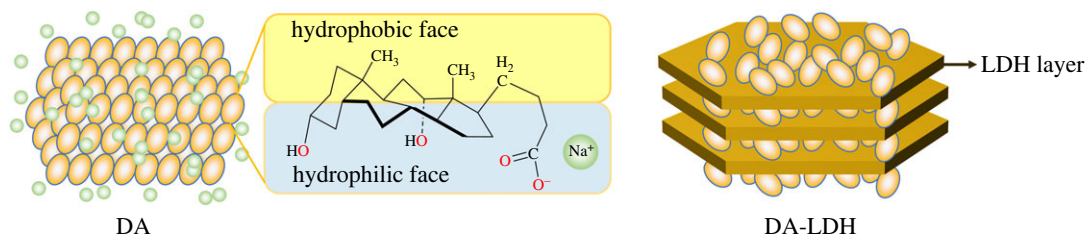


**Figure 1.** Schematic illustrations of DA crystal, molecular structure of DA and DA molecules arranged on LDH (DA-LDH).

one of the emerging issues in drug research. Due to the different intermolecular interactions and molecular arrangement, polymorphism influences various properties of drugs, such as dissolution, solubility, stability and hygroscopicity, drug efficacy, bioavailability, etc. [1–6]. Acetaminophen, one of the well-known painkiller drugs, was reported to show different compressibility behaviour during fabrication depending on the polymorphism [7]. Some drug molecules acquire additional thermodynamic stability due to the optimized intermolecular interaction [8,9]. It was also reported that the suppressed molecular interaction in a confined space resulted in a formation of a certain structure or a specific chemical reaction. Incorporation of amino acid molecules between the two-dimensional layered materials facilitated its polymerization [10,11]. Similarly, oligomerization of ribonucleotide was catalysed by the molecular arrangement in the interlayer space of clay material [12]. Furthermore, confinement of guanosine molecules in the interlayer space of layered metal hydroxide drove the formation of a certain supramolecular assembly through facilitated hydrogen bonding [13].

One of the target substances to control molecular interaction for practical application is deoxycholic acid (DA). It is a naturally occurring amphiphilic molecule; in the living system, DA is found in bile acid and involved in the dissolution metabolism of fat. Due to its surfactant-like chemical nature and low toxicity, DA has been widely studied in cholesterol solubilization, dietary fat manufacturing, fat-soluble vitamin absorption, etc. [14–16]. Although DA has a versatile fat-dissolving role inside the biological system, its application *ex vivo* has been restricted due to its uncontrollable molecular interaction. Different from conventional chemical surfactants, which have a small polar head and a long hydrophobic tail, DA consists of a flat structure with hydrophilic and hydrophobic sides at each face (figure 1) [17,18]. Due to this structural property, DA sensitively forms aggregates at low pH, at improper temperature, or under imbalanced solvent conditions. In order to expand the application spectrum of DA, there have been several approaches to comprehend its molecular interaction. Like other surfactants, it has been reported that the solvent composition affected the molecular aggregation of DA. According to Das *et al.* the critical micellar concentration of DA increased—the molecular aggregation of DA tended to be prevented—as ethylene glycol was added to the aqueous DA solution [19]. As reported in other surfactants such as cetyltrimethylammonium bromide or tetradecyltrimethylammonium bromide, [20] the addition of low surface tension solvent can reduce the molecular interaction, resulting in increased critical micellar concentration. On the other hand, the existence of a certain additive was known to accelerate aggregation of DA moiety. Amino acids, such as lysine, arginine and histidine, were reported to reduce the critical aggregation concentration of DA [21]. It was inferred that both electrostatic and hydrophobic interactions between DA and amino acids collect the DA moieties more tightly to facilitate molecular aggregation. Incorporation of DA with layered inorganic materials such as layered double hydroxide (LDH) can be suggested as a strategy to control the aggregation of DA, allowing effective, versatile application of DA. There have been several approaches to incorporating DA moiety into LDHs; however, most of the studies used complicated or energy-consuming synthetic routes. For example, Ogawa *et al.* intercalated deoxycholic acid into LDH through a hydrothermal reaction, resulting in the topotactically expanded particle thickness of LDH toward *c*-axis [22]. On the other hand, Wu *et al.* intercalated DA into LDH nanohybrids via exfoliation of LDH and the co-assembly arrangement of LDH and DA [23]. Both studies were successful in preparing DA intercalated LDH; however, the DA moiety is inevitably subjected to harsh physical and chemical circumstances during synthesis. Hydrothermal condition accompanies high temperature and pressure; the organic moiety encounters formamide—a strong amphiphilic solvent—during the exfoliation-reassembly process. Our purpose is to find the most effective and simple way to accommodate DA moiety into LDH through general synthetic routes such as coprecipitation, ion exchange or reconstruction.

In this study, we are going to suggest a method to control the molecular arrangement of DA using inorganic material. It was previously reported that the organic molecules could be aligned at the surface of inorganic materials, possibly through adsorption or electrostatic interaction, and that the

preferred orientation of molecules can alter the physicochemical properties of the molecules. For instance, methyl orange dyes were incorporated in the interlayer space of layered metal hydroxide to have modified excitation-emission wavelength [24]. Electrostatic interaction between molecules and inorganic particles arranges the organic molecules to control the light absorption-emission property of luminescent species [25]. Inorganic particles could also stabilize vulnerable organic molecules to make bulk-like stability but single-molecule-like photophysical properties [26]. In addition, the confinement of benzene molecules in the pore channel of MCM-41 reduced its diffusion coefficient due to the modified molecular orientation [27]. Taking into account the previous research, we tried to incorporate DA molecules in the interlayer space of LDH. The LDH, of which chemical formula is expressed as  $[M(II)_{1-x}M(III)_x(OH)_2]^{x+} (A^{n-})_{x/n}$  (M: metal, A: anion) consists of positively charged nanolayers and electrostatically stabilized interlayer anions [28–30]. As the LDH layer provides periodic positive charge as well as large layer, we hypothesized that the incorporation of DA into LDH resulted in the arrangement of molecules in a two-dimensional and controlled manner, which is illustrated in figure 1. In addition, the molecular interaction, which was governed by the inter-molecular van der Waals force, would be regulated by the DA-LDH electrostatic interaction. The point of this study is how to incorporate DA into LDH by overcoming the strong inter-molecular interaction. In order to answer this question, we approached the three well-known intercalation methods in LDH, coprecipitation, ion-exchange and reconstruction. The interaction between DA molecules and LDH layers, depending on the incorporation methods, will be discussed in terms of crystal structure, chemical bonding, microstructure and molecular interaction.

## 2. Material and methods

### 2.1. Material

The DA sodium salt with more than 98% purity was purchased from Sigma-Aldrich LLC, MO, USA. Magnesium nitrate hexahydrate ( $Mg(NO_3)_2 \cdot 6H_2O$ ), aluminium nitrate nonahydrate ( $Al(NO_3)_3 \cdot 9H_2O$ ), sodium hydroxide (NaOH), sodium bicarbonate ( $NaHCO_3$ ) and sodium nitrate ( $NaNO_3$ ) were all purchased from Daejung Co. Ltd., Korea. All the reagents were used as purchased.

### 2.2. Incorporation of DA into LDH

In order to incorporate DA into LDH through coprecipitation (DL-C), 0.015 mol of DA was first dissolved in 200 ml of decarbonated water. Then, a solution containing 0.03 mol of  $Mg(NO_3)_2 \cdot 6H_2O$  and 0.01 mol of  $Al(NO_3)_3 \cdot 9H_2O$  was added to the DA solution. The mixture was then titrated with  $1 \text{ mol l}^{-1}$  of NaOH solution to reach a pH of approximately 9.5. The reaction vessel was kept for 1 day under nitrogen bubbling in order to avoid undesired contamination by atmospheric carbon dioxide. The white precipitate was separated by centrifugation and washed with decarbonated water three times.

For the synthesis of DA-LDH through ion exchange (DL-I), the pristine LDH was prepared in advance. An aqueous solution containing  $0.2 \text{ mol l}^{-1}$  of total metal concentration (ratio of  $Mg(NO_3)_2 \cdot 6H_2O$  over  $Al(NO_3)_3 \cdot 9H_2O$  was set 3) was prepared in decarbonated water and titrated with  $1 \text{ mol l}^{-1}$  NaOH solution up to pH approximately 9.5. In order to avoid carbonate contamination, the reaction was carried out under nitrogen bubbling, and  $NaNO_3$  solution ( $0.12 \text{ mol l}^{-1}$ , 100 ml) was added during titration. The white suspension was kept for 1 day under vigorous stirring and nitrogen bubbling. The white precipitate, MgAl-NO<sub>3</sub>-LDH, was collected by centrifugation and washed with decarbonated water three times. The precipitate was then resuspended in decarbonated water and mixed with DA solution ( $0.1 \text{ mol l}^{-1}$ ). The molar ratio of Al in LDH and DA was set at 1:3 (Al:DA). The mixed suspension was incubated for 1 day under vigorous stirring and  $N_2$  bubbling. The final precipitate was separated by centrifugation and washed with decarbonated water three times.

The DA-LDH made by reconstruction (DL-R) was prepared as follows. First, MgAl-CO<sub>3</sub>-LDH was prepared as described in MgAl-NO<sub>3</sub>-LDH. Both decarbonated water and sodium nitrate were replaced by deionized water and sodium bicarbonate, respectively, for the MgAl-CO<sub>3</sub>-LDH synthesis. The lyophilized MgAl-CO<sub>3</sub>-LDH was thermally treated in a muffle furnace at 600°C for 12 h. Thus, obtained metal oxide (0.5 g) was dispersed in a DA solution ( $0.05 \text{ mol l}^{-1}$ , 200 ml). The mixture was reacted for 1 day under  $N_2$  bubbling. The final precipitate was separated by centrifugation and washed with decarbonated water three times.

All three DL hybrids were lyophilized and ground in an agate mortar to get fine powder.

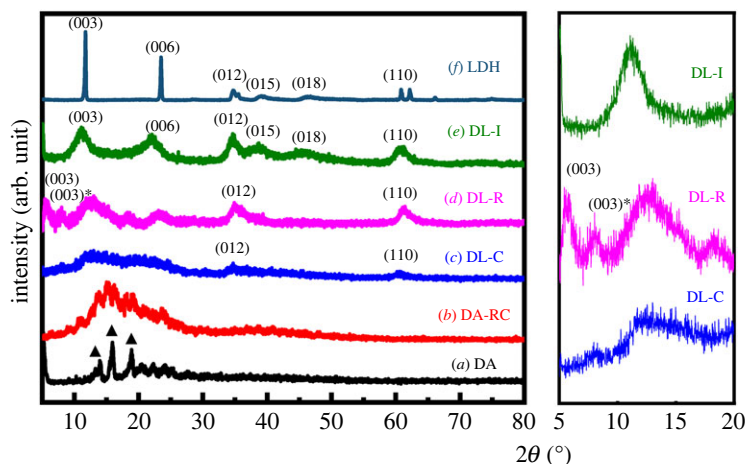


**Figure 2.** Powder X-ray diffraction patterns of (a) DA, (b) DA-RC, (c) DL-C, (d) DL-R, (e) DL-I and (f) LDH. The right panel is a magnified diffractogram of three DA-LDH hybrids, DL-C, DL-R and DL-I, in low angle region. The two peaks of DL-R in low angle regions may be two (003) peaks from different interlayer spaces; they are denoted as (003) and (003)\* for clarification.

### 2.3. Characterization

Structural characterizations for DA and LDHs with DA were carried out with X-ray diffraction (XRD) and Fourier-transform infrared (FT-IR) spectroscopy. The XRD patterns were collected in the  $2\theta$  range from  $5^\circ$  to  $80^\circ$  with time-step increments of  $0.02^\circ$  and 0.5 s per step. The XRD patterns were obtained with Ultima IV (Rigaku, Tokyo, Japan) by using Ni-filtered Cu-K $\alpha$  radiation ( $\lambda = 1.5409 \text{ \AA}$ , 40 kV, 30 mA) as an X-ray source. The FT-IR spectra were recorded using an FT/IR-4600 spectrometer (JASCO, Tokyo, Japan) in the range (2000–600)  $\text{cm}^{-1}$ , with 4  $\text{cm}^{-1}$  resolution, to detect transmission at room temperature. The spectrometer was equipped with an attenuated total reflectance (ATR) accessory and Ge crystal. The powders of DA and LDH with DA were placed on the crystal and directly measured via ATR. The morphology of the DA and LDH with DA were visualized by scanning electron microscopy (SEM) with JSM-6700F (JEOL, Tokyo, Japan). The measured sample was prepared by carefully spreading the powder on carbon tapes. Particle sizes, morphologies and the crystallographic arrangement of the LDHs were observed under field emission transmission electron microscope (FE-TEM: JEM-F200, JEOL) with an accelerating voltage of 200 kV. The TEM samples were prepared by placing drops of ethanol suspension of LDHs onto carbon-coated copper grids with a 200 mesh. After the sample settlement, the grids were dried in air to remove the solvent for 1 h. Thermal analysis was conducted using differential scanning calorimetry (DSC) of Jade DSC (PerkinElmer, Inc., WA, USA) set for scanning from 20 to  $400^\circ\text{C}$  at  $10^\circ\text{C}/\text{min}$  under nitrogen atmosphere. Hydrodynamic radii of LDH and DA-LDH suspension at a concentration of  $1 \text{ mg ml}^{-1}$  in water were measured by dynamic light scattering (DLS) with ELSZ-1000 (Otsuka electronics, Hirakata, Japan).

## 3. Results and discussion

### 3.1. Crystal structure

The crystal structure of three DA-LDH and DA only were investigated with powder X-ray diffraction, as shown in figure 2. It was clearly demonstrated that the sodium salt of DA had a crystalline structure (figure 2a) as reported in the previous literature [31,32]. It was known that the crystalline DA became amorphous by dehydration and recovered crystallinity upon appropriate hydration [31]. The fact suggests that the aggregation of DA molecules is fairly strong and reversible in the existence of water molecules. We also observed aggregation and crystallization of DA after sequential dissolution and precipitation. Sample DA-RC, of which XRD pattern was represented in figure 2b, was prepared by treating Na-DA solution with  $1 \text{ mol l}^{-1}$  hydrochloric acid. The clear Na-DA solution readily turned to white precipitates along with crystallization of molecules. Although the X-ray diffractogram of DA-RC was generally amorphous (figure 2b), it still exhibited representative peaks of DA crystal in the  $2\theta$  range  $10\text{--}20^\circ$ .

The sharp crystalline peaks, which are typical features of salt, became broad upon reaction with LDH. The hybrid obtained by direct coprecipitation (DL-C) showed almost amorphous diffraction pattern with

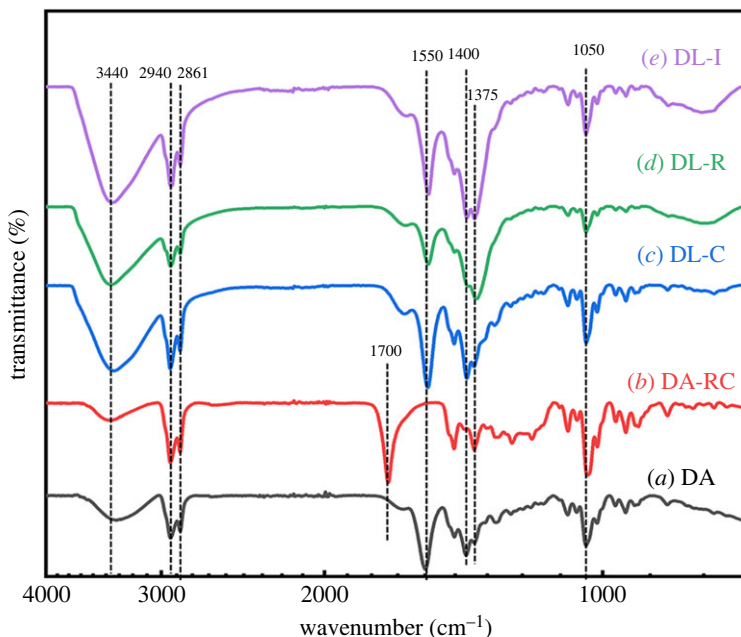


**Figure 3.** FT-IR spectra of (a) DA, (b) DA-RC, (c) DL-C, (d) DL-R and (e) DL-I.

two small peaks at around  $2\theta = 35^\circ$  and  $60^\circ$  attributed to (012) and (110) reflection of LDH lattice (figure 2c). The absence of (001) peaks in the diffractogram of DL-C, as well as the small lattice peaks, suggested that small LDH crystallites were precipitated in the presence of DA. Although we could not observe the evidence that DA molecules were intercalated into LDH layers in DL-C, it could be at least proposed that small LDH crystallites restrain inter-molecular crystallization of DA moiety. The figure 2d and the corresponding magnified diffractogram for DL-R—the hybrid obtained by reconstruction—clearly showed both (001) peaks and lattice peaks of LDH. DL-R was obtained by the calcination of the LDH intercalated with carbonate anions and reconstruction of LDH in the existence of deoxycholate anions. It was noteworthy that DL-R exhibited two peaks in the low angle region, at  $2\theta$  values of  $5.5^\circ$  and  $8.1^\circ$ , respectively. Compared with pristine LDH (figure 2f), the (003) peaks shifted from  $11.3^\circ$  to the lower angle region, indicating that the deoxycholate anions were located in the interlayer gallery of LDH. In addition, the d-spacing of the two peaks at  $2\theta$  values of  $5.5^\circ$  and  $8.1^\circ$  corresponded to 1.60 nm and 1.09 nm, respectively. It was noteworthy that DL-R exhibited two peaks in low angle region, at  $2\theta$  value  $5.5^\circ$  and  $8.1^\circ$ , respectively. The d-spacing of the two peaks corresponded to 1.60 nm and 1.09 nm, respectively. The two peaks can be interpreted as a set of (001) peaks—(006) and (009)—or two (003) peaks from different interlayer spacings. The former interpretation hypothesized (003) peak at  $2.7^\circ$  with the d-spacing of 3.21 nm, possibly forming double layer orientation of DA in the interlayer space. According to the latter interpretation, two different d-spacings of 1.60 nm and 1.09 nm existed in the sample depending on the tilting angle of DA moiety in a single-layer manner. The discussion on the interlayer arrangement will be clarified in the high-resolution transmission electron microscopy part. In either case, the interlayer space expanded sufficiently large to accommodate DA molecules between LDH layers. Unfortunately, the DL-I, the hybrid prepared by ion exchange reaction, did not show any evidence of DA intercalation. The diffractogram only exhibited signals from pristine LDH, suggesting that DA moieties were simply adsorbed at the surface of LDH rather than incorporated into LDH on a nanometer scale. It could be therefore concluded that either coprecipitation or reconstruction was effective in getting homogeneous combination of DA and LDH in the nanoscopic dimension. Between the two methodologies, reconstruction was determined to be the more efficient for separating DA molecules by using nanospace of LDH interlayer; two-dimensional arrangement of DA molecules in DL-R would restrict their molecular aggregation.

In order to further inspect the DA moiety incorporated with LDH, the chemical structure of DA moiety with LDH at each state was examined by FT-IR spectroscopy. The chemical structure of DA moiety at each state was examined by FT-IR spectroscopy. As shown in figure 3, all the materials showed characteristic peaks of DA backbone at around  $1375\text{ cm}^{-1}$  and  $1050\text{ cm}^{-1}$ , which attributed to  $-\text{CH}_3$  and  $-\text{CCO}^-$  functional groups, [23,33,34] suggesting that the intact structure of DA did not

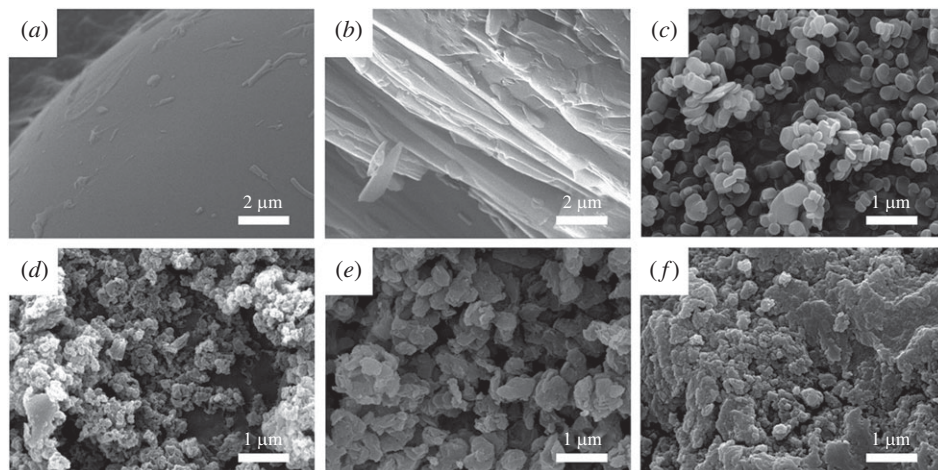


**Figure 4.** SEM images of (a) DA, (b) DA-RC, (c) LDH, (d) DL-C, (e) DL-R and (f) DL-I.

change upon recrystallization nor hybridization with LDH. The wide band at  $3440\text{ cm}^{-1}$  for all the samples was attributed to the symmetric and antisymmetric O–H stretching modes of DA and interlayer water molecules of LDH or surface absorption water [35–37]. It could also be noted that the asymmetric and symmetric methylene stretching bands of DA were  $2940\text{ cm}^{-1}$  and  $2861\text{ cm}^{-1}$ , respectively [35,38]. Different from the other samples, DA-RC, which is the recrystallized DA upon acid treatment, showed clear peaks at around  $1700\text{ cm}^{-1}$  due to the existence of carboxylic acid (–COOH) groups. It was expected that the sudden addition of hydronium ion in Na-DA solution gave rise to protonation of carboxylate moiety, reducing the quantity of  $\text{Na}^+\text{–COO}^-$  ionic bond. As expected, all the four spectra except DA-RC showed two peaks at around  $1550\text{ cm}^{-1}$  and  $1400\text{ cm}^{-1}$ , which was originated from antisymmetric and symmetric stretching of carboxylate (–COO<sup>–</sup>) moiety, respectively [39–41]. The results suggested that all the three hybrids contained DA molecules and that the DA well preserved their carboxylate moiety, facilitating the charge-charge interaction between DA (negative charge) and LDH layers (positive charge), as suggested in the schematic diagram in figure 1.

### 3.2. Particle morphology

The overall morphology of the samples was examined on a microscopic scale. As shown in figure 4a, the DA itself showed very large lumps of particles, of which the surface was smooth. The large lump is strongly related to the high crystalline phase of DA in XRD (figure 2), indicating that the intermolecular aggregation was strong. The recrystallized DA (DA-RC) also showed large lumps; however, the feature was fairly different from DA alone (figure 4b). It was recently reported that the Na-DA could aggregate in various forms, including rods, sponges, vesicles, lamellae, bundles of tubes, etc. [42]. Similar to the conventional surfactants, which form micelle, hexagonal array and lamellar structure depending on the concentration, the DA molecules gathered into lamellar or tubular morphology. In the process of DA-RC formation, the rapid increase in hydrophobicity might accelerate the strong intermolecular interaction through one-dimensional or two-dimensional direction, to form such a lamellar or needle-like morphology. The SEM images of three hybrids were different from that of DA or DA-RC. All the samples showed particles of less than  $1\text{ }\mu\text{m}$ , which corresponded to the dimension of LDH particles (figure 4c). This clearly showed that the crystalline nature of DA was highly suppressed after the reaction with LDH, although the detailed feature of DA would be different according to the hybridization method. As shown in figure 4d, the DL-C, the coprecipitated hybrid, showed smaller particles compared with the other hybrids. The small particle size was attributed to the low crystallinity, as shown in the XRD (figure 2c). The DL-R had a relatively larger particle size than the other hybrids and did not show specific morphology (figure 4e). This is a typical morphology of LDH after reconstruction with organic moiety [43–45]. As the layer-by-layer stacking is slightly disordered in the reconstruction reaction, the particles of organically reconstructed LDH tended to show a random assembly of lamellar sheets. The SEM image of DL-I exhibited relatively inhomogeneous and irregular particles (figure 4f). Considering that the DL-I showed crystalline peaks corresponding to LDH (figure 2e), the small size and irregularity of particle in SEM image are not expected features. The discrepancy can be explained by the surface-adsorbed organic moieties. The

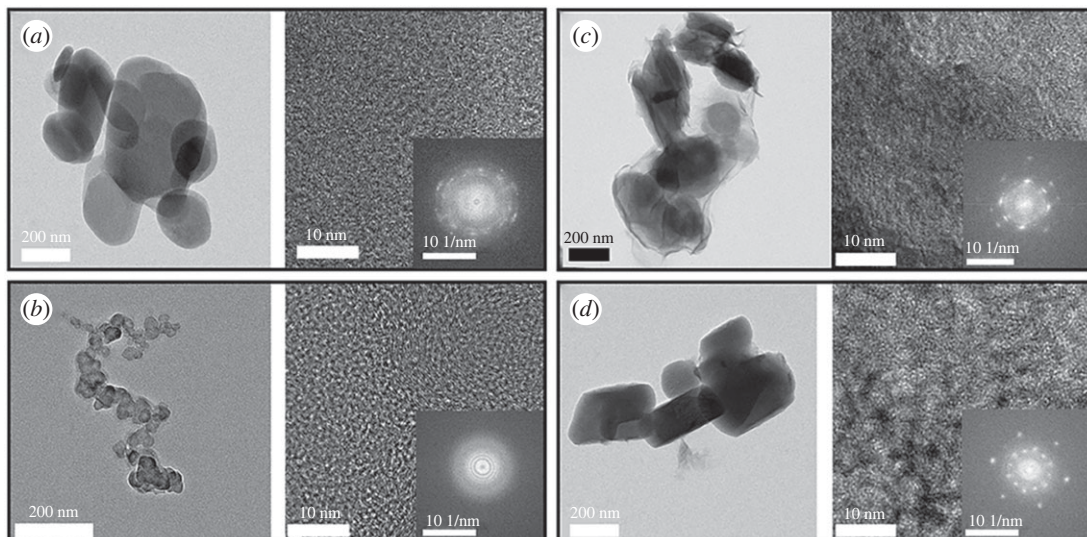


**Figure 5.** TEM images and corresponding fast Fourier transforms (FFT) patterns of (a) LDH, (b) DL-C, (c) DL-R and (d) DL-I.

LDH particles did not accommodate DA moiety in their interlayer space but adsorb at the surface. The DA molecules then aggregated on the LDH surface to camouflage the morphology of LDH. The organic moiety at the surface of LDH hides the crystalline particles, resulting in the irregular surface morphology.

In order to investigate the intracrystalline structure of DL hybrids in detail, transmission electron microscopy (TEM) was carried out to obtain images and fast Fourier transform (FFT) patterns (figure 5). As shown in the electronic supplementary material, figure S1, the organic moiety, such as DA itself and recrystallized DA (DA-RC), were unstable under electron beam irradiation; the TEM did not show images of typical crystalline material. The particle sizes of LDH, DL-C, DL-R and DL-I were statistically measured by selecting at least 20 particles from TEM images and compared through Student *t*-test (electronic supplementary material, figure S2 and table S1). The mean particle sizes of LDH, DL-C, DL-R and DL-I were calculated to  $219 \pm 63$  nm,  $34 \pm 8$  nm,  $213 \pm 46$  nm and  $218 \pm 70$  nm, respectively, revealing that there was no significant particle size difference among LDH, DL-R and DL-R. The result suggested that the reactions in ion exchange and reconstruction occurred in a topotactical manner maintaining particle diameter. The reason why DL-C showed significantly small particle size was the different synthetic approach. In the coprecipitation, the LDH particles were grown *in situ* with the arrangement of DA molecules. The small particle size of DL-C corresponded to its low crystallinity reflected by the ring pattern in FFT. The pattern represented that the DL-C hybrids had amorphous-like structure for both inorganic (LDH) and organic (DA) moiety. This result corresponded to the XRD pattern (figure 2c), in which only a few crystalline peaks corresponding to the lattice of LDH were found. The DL-R showed a well-defined image of particles. Although the particle size and the particle shape of LDH and DL-R were similar, there were no distinct particle edges of DL-R shown in figure 5c and electronic supplementary material, figure S3, proposing that the highly ordered-layered structure of LDH was absent after reconstruction attributed to the intercalation of DA moieties. As we discussed in the SEM part, the fluffy moiety is the LDH layer that lost the ordering of layer-by-layer stacking during reconstruction process. Based on the morphological change and the clear hexagonal spot patterns in FFT of DL-R (figure 5c), we could expect that the LDH layers were maintained and the organic/inorganic hybridization homogeneously occurred at a nanoscopic level. The TEM image of DL-I showed a typical feature of inorganic particles except for the existence of a grey contrast part outside of the particle. Furthermore, the FFT pattern of DL-I was almost same as that of conventional LDH, suggesting that there was no change in LDH part after the reaction. Thus, we expected that the ion exchange reaction was not enough to induce organic-inorganic nanohybrid and that the inorganic part (LDH) and organic part (DA) existed with phase separation. To summarize, the DL-R hybrid had the most periodic hybridization between DA and LDH in nanoscale among the three hybrids. In addition, the DL-C had an amorphous mixture of DA and LDH, which may not take advantage of LDH layers to the direct molecular arrangement. Further, the DL-I did not induce significant molecular arrangement change of DA moiety. Taking into account the XRD, SEM and TEM results, we could suggest the schematic diagram of DA arrangement as

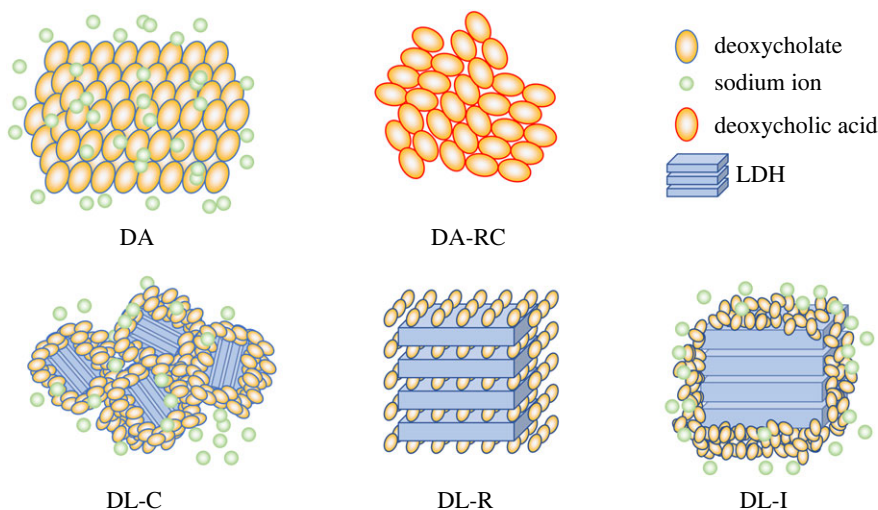


**Figure 6.** Schematic structures of DA powder (DA), recrystallized DA (DA-RC), and the three hybrids obtained by coprecipitation (DL-C), reconstruction (DL-R) and ion-exchange (DL-I).

illustrated in figure 6. The crystal of DA had highly ordered arrangement DA, while the recrystallized DA (DA-RC) had aggregation with relatively low crystallinity due to the sudden growth of crystal. In the three DL hybrids, both DA-C and DA-I did not successfully accommodate DA moiety into the structure but adsorbed DA on the surface. On the other hand, DL-R is considered to arrange DA moiety in the most ordered manner by confining the organic moiety in the two-dimensional space.

### 3.3. Interlayer arrangement

As it was suggested by the XRD and TEM that DL-R hybrid has the most ordered orientation of DA moiety along the *ab*-plane among the DL hybrids, we further investigated the layer-by-layer arrangement of the hybrid by using HR-TEM and electron density histogram. Figure 7*a* exhibited the magnified image of a DL-R hybrid, which happened to orient perpendicular to the *c*-axis. We could clearly observe the assembly of lines, which was attributed to the layer stacking of LDHs. The electron density histogram along the *c*-axis, which was taken from a set of line assemblies in HR-TEM image, was displayed in figure 7*b*. The electron density peaks were regularly arranged with 1.6 nm or 1.1 nm distances. From the XRD patterns, we expected either (i) a double-layer arrangement of DA with 3.21 nm *d*-spacing or (ii) a single-layer arrangement with two different tilting states with 1.60 and 1.09 nm. The electron histogram clearly showed that the latter interpretation was correct. As suggested in figure 7*c*, DA molecules can be arranged in the interlayer space with tilted or horizontal orientation, depending on the intermolecular attraction and the organic-inorganic interaction. Since LDHs have positively charged metal hydroxide layers and anions in the interlayer gallery, DA molecules as anionic organic species could interact with LDH by periodic electrostatic affinity when a proper synthetic condition is applied [22,23].

As we confirmed that the three-dimensional assembly of DA was rearranged to the two-dimensional direction in the DL-R hybrid, we further investigated the intermolecular attraction in DA moiety using the DSC technique. The DA as it is showed one distinct exothermic peak at 184°C and two endothermic peaks at 235 and 353°C, respectively (figure 8*a*). According to the previous literature, deoxycholic acid showed various behaviours with respect to temperature [46–49]. Some papers reported the endothermic behaviour of DA at around 200°C due to melting; [46,47] other papers observed step-by-step exothermic and endothermic behaviours upon temperature increase [48]. Different thermal behaviours of DA may be attributed to the various molecular arrangements resulting from the strong intermolecular interaction. As reported previously, [49] the exothermic peak at around 180°C was attributed to the recrystallization, and the endothermic reactions were related to the intermolecular separation—melting. The DSC diagram of recrystallized DA-RC was slightly different from that of DA alone. As displayed in figure 8*b*, we could observe sharp endothermic peaks at 103°C, 173°C, 297°C and a broad endothermic phenomenon at around 350°C. The first endothermic reaction at 103°C was attributed to dehydration, as the sample contained lots of water moiety during

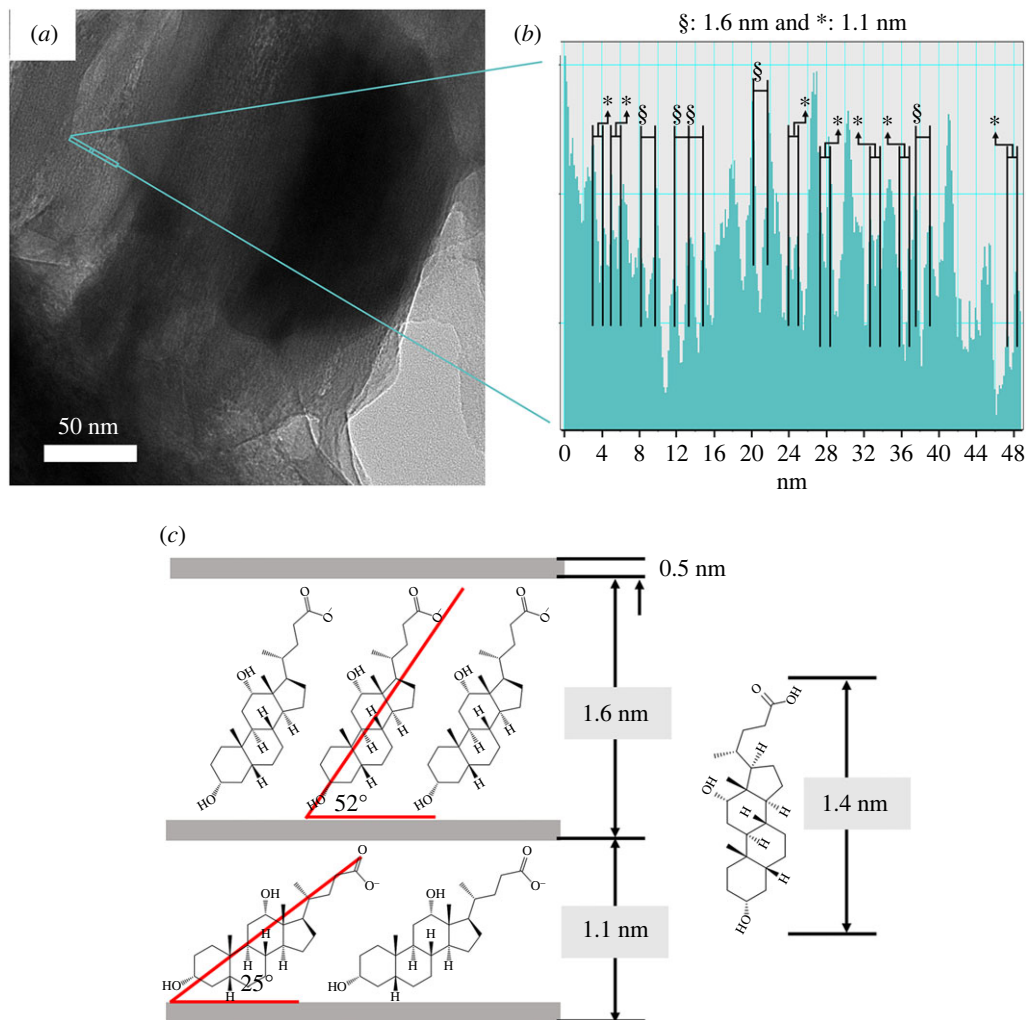


**Figure 7.** (a) TEM image and (b) the histogram obtained from a green rectangle in TEM for visualizing interlayer distance of DL-R. (c) Schematic illustration on the interlayer arrangement of DA moiety in LDH.

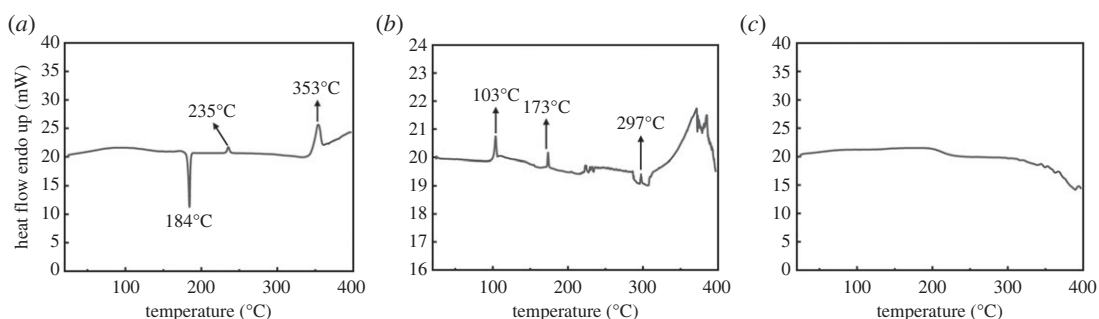


**Figure 8.** DSC curves of (a) DA, (b) DA-RC and (c) DL-R.

the recrystallized process. The sharp endothermic peaks of DA-RC at 173°C and 297°C corresponded to those of DA alone at 184°C and 235°C. As the recrystallization was carried out rapidly, the DA molecules did not have enough time to fully aggregate themselves. Thus, the molecular separation—melting—of DA-RC occurred at a lower temperature than DA alone. Anyway, both DA and DA-RC, which are thought to have molecular interaction in a three-dimensional direction, exhibited discrete exothermic or endothermic behaviours due to the active intermolecular attractions. On the other hand, the DSC diagram of DL-R, the reconstructed DA-LDH hybrid, did not show heat flow until 350°C (figure 8c). This result implied that there was restricted molecular interaction of DA in the DL-R hybrid. The molecular arrangement of DA between the LDH layers was more governed by the charge-charge

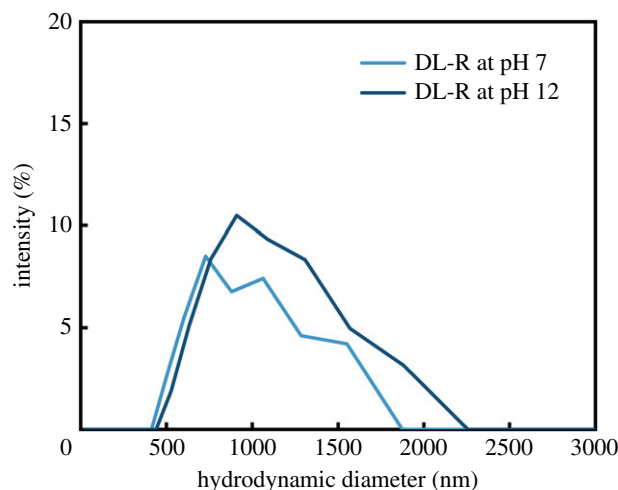


**Figure 9.** DLS size distribution by intensity of the DL-R prepared at pH 7 and pH 12 in water and pH adjusted by using 1 M of NaOH.

interaction between DA and LDH than the molecule-molecule interaction. It is therefore concluded that the strong and uncontrolled molecular aggregation of DA could be suppressed through molecular rearrangement in between the LDH layer by the reconstruction reaction.

The stability of DL-R in both neutral (pH 7) and basic (pH 12) media was monitored through DLS. The hydrodynamic diameters of DL-R in pH 7 aqueous condition presented a similar particle size distribution to that of DL-R in pH 12 aqueous suspension, as shown in figure 9. The particle sizes of DL-R remained unchanged even under strong base conditions, as the LDH protected the payloads from basic condition. As the LDH moiety can be soluble in acidic media, the colloidal stability of DA-LDH in acidic condition may be different from that in neutral pH. However, it can be suggested that the dissolution of LDH in acidic media plays a buffering role in protecting DA moiety from the attack of acid [50,51].

DA has been used to reduce submental fat [52,53] and play a role in the emulsion as emulsifiers [54,55] to enhance the stability of immiscible liquids. However, there have been detrimental issues of DA, such as strong aggregation in certain media, resulting in the loss of functionality. The incorporation of DA in the LDH interlayer space could avoid molecular aggregation due to the formation of an inorganic layered network surrounding DA molecules. Once stabilized DA can effectively perform its inherent functions, such as an emulsifier, a fat dissolver, etc. in a variety of media. Indeed, the DA-LDH could be used in the formulation of oil in water emulsion [50], which can be further used as cosmetics for transdermal delivery platforms.

## 4. Conclusion

The DA molecules were incorporated into the interlayer space of LDH through three synthetic strategies in order to control the molecular arrangement. Conventional coprecipitation resulted in the development of small crystallites of LDH, resulting in the coexistence of both LDH particles and DA crystals. Although the crystallinity of DA decreased after coprecipitation with LDH, the method was not efficient in arranging DA molecules in a preferred manner. The ion-exchange reaction between the DA solution and MgAl-NO<sub>3</sub>-LDH resulted in no change in crystal structure, resulting in the surface adsorption of DA moiety. The crystallinity of DA decreased after the ion-exchange reaction; however, we did not consider this method practical as the surface adsorbed amount would be very low. On the other hand, the reconstruction method, in which DA solution and metal oxide reacted together, gave rise to the well-ordered DA moieties in between the LDH layers. The X-ray diffraction and FT-IR spectroscopy indicated that the DA molecules were well stabilized through electrostatic interaction between DA and LDH and that the molecules were tilted by 25° or 52°, minimizing intermolecular interaction over DA-LDH attraction. The HR-TEM images and electron-density line profile clearly showed that the DA molecules were preferentially arranged in two-dimensional direction when DA and LDH were hybridized through the reconstruction method. Finally, the DSC curves confirmed that

there was no significant intermolecular attraction among DA, when the molecules were incorporated into LDH through the reconstruction reaction.

**Ethics.** An ethical statement is not relevant for this study as no animal work has been carried out.

**Data accessibility.** Data that support this study have been uploaded as part of the electronic supplementary material [56]. In addition, the datasets can also be found at <https://doi.org/10.5061/dryad.q2bvq83qk> [57].

**Declaration of AI use.** We have not used AI-assisted technologies in creating this article.

**Authors' contributions.** K.L.: data curation, formal analysis, investigation, methodology, validation, visualization, writing—original draft; J.X.: data curation, formal analysis, investigation, methodology, writing—original draft; H.P.: formal analysis, investigation, methodology, visualization; H.J.: conceptualization, funding acquisition, project administration, supervision, writing—review and editing; J.-M.O.: conceptualization, funding acquisition, project administration, supervision, writing—review and editing.

All authors gave final approval for publication and agreed to be held accountable for the work performed therein.

**Conflict of interest declaration.** We declare we have no competing interests.

**Funding.** This research was supported by the National Research Foundation of Korea (NRF) funded by the Korean government (MSIT) (no. NRF-2022R1F1A1064008 and NRF-2020R1F1A1073107).

## References

- Raza K, Kumar P, Ratan S, Malik R, Arora S. 2014 Polymorphism: the phenomenon affecting the performance of drugs. *SOJ Pharm Pharm Sci.* **1**, 1–10.
- Chistyakov D, Sergeev G. 2020 The polymorphism of drugs: new approaches to the synthesis of nanostructured polymorphs. *Pharmaceutics* **12**, 34. (doi:10.3390/pharmaceutics12010034)
- Ayala AP. 2007 Polymorphism in drugs investigated by low wavenumber Raman scattering. *Vib. Spectrosc.* **45**, 112–116. (doi:10.1016/j.vibspec.2007.06.004)
- Kerb R. 2006 Implications of genetic polymorphisms in drug transporters for pharmacotherapy. *Cancer Lett.* **234**, 4–33. (doi:10.1016/j.canlet.2005.06.051)
- Higuchi W, Lau P, Higuchi T, Shell J. 1963 Polymorphism and drug availability. Solubility relationships in the methylprednisolone system. *J. Pharm. Sci.* **52**, 150–153. (doi:10.1002/jps.2600520210)
- Zhou Y, Wang J, Xiao Y, Wang T, Huang X. 2018 The effects of polymorphism on physicochemical properties and pharmacodynamics of solid drugs. *Curr. Pharm. Des.* **24**, 2375–2382. (doi:10.2174/1381612824666180515155425)
- Nichols G, Frampton CS. 1998 Physicochemical characterization of the orthorhombic polymorph of paracetamol crystallized from solution. *J. Pharm. Sci.* **87**, 684–693. (doi:10.1021/js970483d)
- Eyjolfsson R. 2002 Enalapril maleate polymorphs: instability of form II in a tablet formulation. *Pharmazie* **57**, 347–348.
- Lin W-Q, Jiang J-H, Yang H-F, Ozaki Y, Shen G-L, Yu R-Q. 2006 Characterization of chloramphenicol palmitate drug polymorphs by Raman mapping with multivariate image segmentation using a spatial directed agglomeration clustering method. *Anal. Chem.* **78**, 6003–6011. (doi:10.1021/ac0520902)
- Whilton NT, Vickers PJ, Mann S. 1997 Bioinorganic clays: synthesis and characterization of amino-andpolyamino acid intercalated layered double hydroxides. *J. Mater. Chem.* **7**, 1623–1629. (doi:10.1039/A701237C)
- Jaber M, Georgelin T, Bazzi H, Costa-Torro F, Lambert J-F, Bolbach GR, Clodic G. 2014 Selectivities in adsorption and peptidic condensation in the (arginine and glutamic acid)/montmorillonite clay system. *J. Phys. Chem. C* **118**, 25 447–25 455. (doi:10.1021/jp507335e)
- Burcar BT, Cassidy LM, Moriarty EM, Joshi PC, Coari KM, McGown LB. 2013 Potential pitfalls in MALDI-TOF MS analysis of abiotically synthesized RNA oligonucleotides. *Origins Life Evol. Biospheres* **43**, 247–261. (doi:10.1007/s11084-013-9334-5)
- Gwak G-H, Kocsis I, Legrand Y-M, Barboiu M, Oh J-M. 2016 Controlled supramolecular structure of guanosine monophosphate in the interlayer space of layered double hydroxide. *Beilstein J. Nanotechnol.* **7**, 1928–1935. (doi:10.3762/bjnano.7.184)
- Mitra S, Dungan SR. 2001 Cholesterol solubilization in aqueous micellar solutions of quillaja saponin, bile salts, or nonionic surfactants. *J. Agric. Food. Chem.* **49**, 384–394.
- Di Ciaula A, Garruti G, Baccetto RL, Molina-Molina E, Bonfrate L, Portincasa P, Wang DQ. 2018 Bile acid physiology. *Ann. Hepatol.* **16**, 4–14. (doi:10.5604/01.3001.0010.5493)
- Mukhopadhyay S, Maitra U. 2004 Chemistry and biology of bile acids. *Curr. Sci.* **87**, 1666–1683.
- Galantini L, di Gregorio MC, Gubitosi M, Travaglini L, Tato JV, Jover A, Mejjide F, Tellini VHS, Pavel NV. 2015 Bile salts and derivatives: rigid unconventional amphiphiles as dispersants, carriers and superstructure building blocks. *Curr. Opin. Colloid Interface Sci.* **20**, 170–182. (doi:10.1016/j.cocis.2015.08.004)
- Natalini B, Sardella R, Gioiello A, Ianni F, Di Michele A, Marinuzzi M. 2014 Determination of bile salt critical micellization concentration on the road to drug discovery. *J. Pharm. Biomed. Anal.* **87**, 62–81. (doi:10.1016/j.jpba.2013.06.029)
- Das S, Thapa U, Ismail K. 2010 Aggregation and adsorption behaviors of sodium deoxycholate in water–ethylene glycol medium. *Bull. Chem. Soc. Jpn.* **83**, 1352–1358. (doi:10.1246/bcsj.20100152)
- Das J, Ismail K. 2009 Aggregation, adsorption, and clouding behaviors of Triton X-100 in formamide. *J. Colloid Interface Sci.* **337**, 227–233. (doi:10.1016/j.jcis.2009.04.094)
- He F, Xu G, Pang J, Han T, Liu T, Yang X. 2012 Effect of amino acids on aggregation behaviour of sodium deoxycholate in solution: a fluorescence study. *Luminescence* **27**, 4–10. (doi:10.1002/bio.1312)
- Ogawa M, Asai S. 2000 Hydrothermal synthesis of layered double hydroxide–deoxycholate intercalation compounds. *Chem. Mater.* **12**, 3253–3255. (doi:10.1021/cm000455n)
- Wu X, Wang S, Du N, Zhang R, Hou W. 2013 Facile synthesis of deoxycholate intercalated layered double hydroxide nanohybrids via a coassembly process. *J. Solid State Chem.* **203**, 181–186. (doi:10.1016/j.jsschem.2013.06.043)
- Costantino U, Coletti N, Nocchetti M, Aloisi GG, Elisei F. 1999 Anion exchange of methyl orange into Zn–Al synthetic hydroxalite and photophysical characterization of the intercalates obtained. *Langmuir* **15**, 4454–4460.
- Ishida Y. 2021 Manipulation of precise molecular arrangements and their photochemical properties on inorganic surfaces via multiple electrostatic interactions. *Bull. Chem. Soc. Jpn.* **94**, 2886–2897. (doi:10.1246/bcsj.20210303)
- Yamaguchi T, Imwiset KJ, Choi MG, Oh J-M, Lee SY, Ogawa M. 2023 Improved quantum yield of thermally activated delayed fluorescence by nanoconfinement in organophilic octosilicate. *Appl. Clay Sci.* **236**, 106882. (doi:10.1016/j.clay.2023.106882)
- Dervin D, O'Malley A, Falkowska M, Chansai S, Silverwood IP, Hardacre C, Catlow CRA. 2020 Probing the dynamics and structure of confined benzene in MCM-41 based catalysts. *Phys. Chem. Chem. Phys.* **22**, 11 485–11 489. (doi:10.1039/D0CP01196G)
- Kim T-H, Lee JY, Xie J, Park JH, Oh J-M. 2022 Topology dependent modification of layered double hydroxide for therapeutic and diagnostic

- platform. *Adv. Drug Delivery Rev.* **188**, 114459. (doi:10.1016/j.addr.2022.114459)
29. Xie J, Yamaguchi T, Oh J-M. 2021 Synthesis of a mesoporous Mg–Al–mixed metal oxide with P123 template for effective removal of Congo red via aggregation-driven adsorption. *J. Solid State Chem.* **293**, 121758. (doi:10.1016/j.jssc.2020.121758)
  30. Choy J-H, Choi S-J, Oh J-M, Park T. 2007 Clay minerals and layered double hydroxides for novel biological applications. *Appl. Clay Sci.* **36**, 122–132. (doi:10.1016/j.clay.2006.07.007)
  31. Ono M, Anzai H, Tozuka Y, Moribe K, Oguchi T, Yamamoto K. 2005 Water vapor adsorption behavior of sodium deoxycholate anhydrous forms. *Chem. Pharm. Bull.* **53**, 180–183. (doi:10.1248/cpb.53.180)
  32. Su Z, Luthra S, Krzyzaniak JF, Agra-Kooijman DM, Kumar S, Byrn SR, Shaliev EY. 2011 Crystalline, liquid crystalline, and isotropic phases of sodium deoxycholate in water. *J. Pharm. Sci.* **100**, 4836–4844. (doi:10.1002/jps.22690)
  33. Kamel HA, Ezzat S, Ahmed MA, Amr AE-GE, Almezizia A, Al-Omar MA. 2020 Modified potentiometric screen-printed electrodes based on imprinting character for sodium deoxycholate determination. *Biomolecules* **10**, 251. (doi:10.3390/biom10020251)
  34. Yang L, Xu Y, Su Y, Wu J, Zhao K, Chen JE, Wang M. 2005 FT-IR spectroscopic study on the variations of molecular structures of some carboxyl acids induced by free electron laser. *Spectrochim. Acta Part A* **62**, 1209–1215. (doi:10.1016/j.saa.2005.04.027)
  35. Guo Y, Wang R, Shang Y, Liu H. 2018 Effects of polymers on the properties of hydrogels constructed using sodium deoxycholate and amino acid. *RSC Adv.* **8**, 8699–8708. (doi:10.1039/C8RA00171E)
  36. Chen L, Sun B, Wang X, Qiao F, Ai S. 2013 2D ultrathin nanosheets of Co–Al layered double hydroxides prepared in l-asparagine solution: enhanced peroxidase-like activity and colorimetric detection of glucose. *J. Mater. Chem. B* **1**, 2268–2274. (doi:10.1039/C3TB00044C)
  37. Zhang G, Wu L, Tang A, Weng B, Atrens A, Ma S, Liu L, Pan F. 2018 Sealing of anodized magnesium alloy AZ31 with MgAl layered double hydroxides layers. *RSC Adv.* **8**, 2248–2259. (doi:10.1039/C7RA11683G)
  38. Ezzeldeen Y, Swidan S, ElMeshad A, Sebak A. 2021 Green synthesized Honokiol Transfersomes relieve the immunosuppressive and stem-like cell characteristics of the aggressive B16F10 melanoma. *Int. J. Nanomed.* **16**, 5693. (doi:10.2147/IJN.S314472)
  39. Zhang Y, Xin X, Shen J, Tang W, Ren Y, Wang L. 2014 Biodegradable, multiple stimuli-responsive sodium deoxycholate–amino acids–NaCl mixed systems for dye delivery. *RSC Adv.* **4**, 62 262–62 271. (doi:10.1039/c4ra13353f)
  40. Terech P, Sangeetha NM, Maitra U. 2006 Molecular hydrogels from bile acid analogues with neutral side chains: network architectures and viscoelastic properties. Junction zones, spherulites, and crystallites: phenomenological aspects of the gel metastability. *J. Phys. Chem. B* **110**, 15 224–15 233.
  41. Song Z, Xin X, Shen J, Zhang H, Wang S, Yang Y. 2016 Reversible controlled morphologies switching between porous microspheres and urchin-like microcrystals for NaDC/RhB self-assembly and their multifunctional applications. *J. Mater. Chem. C* **4**, 8439–8447. (doi:10.1039/C6TC02329K)
  42. Jover A, Fraga F, Mejjide F, Tato JV, Cautela J, Del Giudice A, di Gregorio MC. 2021 Revealing the complex self-assembly behaviour of sodium deoxycholate in aqueous solution. *J. Colloid Interface Sci.* **604**, 415–428. (doi:10.1016/j.jcis.2021.06.140)
  43. Jeung D-G, Kim H-J, Oh J-M. 2019 Incorporation of glycine max merrill extract into layered double hydroxide through ion-exchange and reconstruction. *Nanomaterials* **9**, 1262. (doi:10.3390/nano9091262)
  44. Kim H-J, Lee S-B, Choi A-J, Oh J-M. 2019 Zingiber officinale extract (ZOE) incorporated with layered double hydroxide hybrid through reconstruction to preserve antioxidant activity of ZOE against ultrasound and microwave irradiation. *Nanomaterials* **9**, 1281. (doi:10.3390/nano9091281)
  45. Jung S-Y, Kim B-K, Kim H-J, Oh J-M. 2021 Development of mesopore structure of mixed metal oxide through albumin-templated coprecipitation and reconstruction of layered double hydroxide. *Nanomaterials* **11**, 620. (doi:10.3390/nano11030620)
  46. Suzuki H, Ogawa M, Hironaka K, Ito K, Sunada H. 2001 A nifedipine coground mixture with sodium deoxycholate. I. Colloidal particle formation and solid-state analysis. *Drug Dev. Ind. Pharm.* **27**, 943–949. (doi:10.1081/ddc-100107675)
  47. Ahmed S, Kassem MA, Sayed S. 2020 Bilosomes as promising nanovesicular carriers for improved transdermal delivery: construction, in vitro optimization, ex vivo permeation and in vivo evaluation. *Int. J. Nanomed.* **15**, 9783–9798. (doi:10.2147/IJN.S278688)
  48. Al-Mahallawi AM, Abdelbary AA, Aburahma MH. 2015 Investigating the potential of employing bilosomes as a novel vesicular carrier for transdermal delivery of tenoxicam. *Int. J. Pharm.* **485**, 329–340. (doi:10.1016/j.ijpharm.2015.03.033)
  49. Ismail A, Teiama M, Magdy B, Sakran W. 2022 Development of a novel bilosomal system for improved oral bioavailability of sertraline hydrochloride: formulation design, in vitro characterization, and ex vivo and in vivo studies. *AAPS PharmSciTech.* **23**, 188. (doi:10.1208/s12249-022-02339-0)
  50. Xie J, Lee K, Park H, Jung H, Oh J-M. 2023 Enhanced emulsifying ability of deoxycholate through dynamic interaction with layered double hydroxide. *Nanomaterials* **13**, 567. (doi:10.3390/nano13030567)
  51. Yang W, Li J, Wang M, Sun X, Liu Y, Yang J, Ng DH. 2020 A colorimetric strategy for ascorbic acid sensing based on the peroxidase-like activity of core-shell Fe<sub>3</sub>O<sub>4</sub>/CoFe-LDH hybrid. *Colloids Surf. B* **188**, 110742. (doi:10.1016/j.colsurfb.2019.110742)
  52. Rzany B, Griffiths T, Walker P, Lippert S, McDiarmid J, Havlickova B. 2014 Reduction of unwanted submental fat with ATX-101 (deoxycholic acid), an adipocytolytic injectable treatment: results from a phase III, randomized, placebo-controlled study. *British J. Dermatol.* **170**, 445–453. (doi:10.1111/bjd.12695)
  53. Farina GA, Cherubini K, de Figueiredo MAZ, Salum FG. 2020 Deoxycholic acid in the submental fat reduction: a review of properties, adverse effects, and complications. *J. Cosmet. Dermatol.* **19**, 2497–2504.
  54. Talele P, Sahu S, Mishra AK. 2018 Physicochemical characterization of solid lipid nanoparticles comprised of glycerol monostearate and bile salts. *Colloids Surf. B* **172**, 517–525. (doi:10.1016/j.colsurfb.2018.08.067)
  55. Han J, Davis SS, Papandreou C, Melia CD, Washington C. 2004 Design and evaluation of an emulsion vehicle for paclitaxel. I. Physicochemical properties and plasma stability. *Pharm. Res.* **21**, 1573–1580. (doi:10.1023/b:pham.0000041451.70367.21)
  56. Lee J, Xie J, Park H, Jung H, Oh JM. 2023 Controlled molecular arrangement of easily aggregated deoxycholate with layered double hydroxide. Figshare. (doi:10.6084/m9.figshare.c.6858282)
  57. Lee J, Xie J, Park H, Jung H, Oh JM. 2023 Data from: Controlled molecular arrangement of easily aggregated deoxycholate with layered double hydroxide. Dryad Digital Repository. (doi:10.5061/dryad.q2bvq83qk)